# Transient simulation of vapor-liquid eruption and overpressure in the drainage terminal of an inclined pipeline during pigging process after water pressure test

Tao Deng, Jun Zhou, Xuan Zhou, Tian Meng, Guangchuan Liang and Jing Gong

## ABSTRACT

Pigging technology is widely used in the oil and gas industry. During the course of pigging, after a water pressure test, the instability of the pig caused by terrain fluctuation can affect the stable operation of the pipeline and even cause burst accidents. This paper describes the four stages of pig movement in an inclined pipeline, with vapor-liquid eruption occuring in the last stage. A hydraulic transient model of the pigging operation after a water pressure test is established based on mass conservation and motion equations, the dynamic equation of the pig, and the vapor-liquid eruption model. The model can simulate the status of fluid flow in the pipeline, track the movement of the pig, and predict the pressure pulses. The simulation results are consistent with the data of two burst accidents, which verifies the correctness of the established model and the reliability of the calculated results. It can therefore provide a reliable and effective theoretical basis for developing a pigging plan on site.

**Key words** | dynamic simulation, pigging operation, pressure pulses, vapor-liquid eruption

**Tao Deng**
China National Petroleum Corporation,
Guangzhou Petroleum Training Center,
Guangzhou,
China

**Jun Zhou** (corresponding author)
**Xuan Zhou**
**Guangchuan Liang**
Southwest Petroleum University,
Chengdu,
China
E-mail: *zhoujunswpu@163.com*

**Tian Meng**
PetroChina Southwest Oil & Gasfield Company,
Chengdu,
China

**Jing Gong**
China University of Petroleum (Beijing),
Beijing,
China

## HIGHLIGHTS

- A hydraulic transient model is established based on mass conservation and motion equations of flow, dynamic equation of pig and vapor-liquid eruption model.
- The model can simulate the fluid flow, the pig movement and the pressure pulses values.
- Results are consistent with the data of two burst accidents.

## NOMENCLATURE

| | | | |
|---|---|---|---|
| $x$ | Distance along the pipeline (m) | $D_e$ | External diameter of the pipeline (mm) |
| $a$ | Acoustic speed of fluid (m/s) | $E$ | Modulus of rigidity of the pipe (MPa) |
| $e$ | The thickness of pipe (m) | $K$ | Bulk modulus of elasticity of the liquid (MPa) |
| $f$ | Friction factor | $H$ | Water head of fluid (m) |
| $g$ | Gravity acceleration ($m{\cdot}s^{-2}$) | $M$ | Pig mass (kg) |
| $m$ | The index number of Darcy formula | $P$ | Pressure (Pa) |
| $t$ | Time (s) | $\alpha$ | Angle between axis and horizontal direction (rad) |
| $A$ | Cross-sectional area of pipeline ($m^2$) | $\beta$ | Volumetric fraction of gas |
| $D$ | Diameter of the pipeline (mm) | $\delta$ | Wall thickness of the pipe (mm) |

doi: 10.2166/ws.2020.316

| | |
|---|---|
| $\nu$ | Kinematic viscosity of liquid ($m^2/s$) |
| $\psi$ | Dimensionless parameter that describes the effect of pipe constraint conditions on the wave speed |
| $\mu$ | Poisson's ratio of the pipe |
| $A_l$ | Cross-sectional area of liquid flow ($m^2$) |
| $A_g$ | Cross-sectional area of gas flow ($m^2$) |
| $f_i$ | Fanning friction factor of gas-liquid interface |
| $f_g$ | Fanning friction factor of gas phase |
| $f_l$ | Fanning friction factor of liquid phase |
| $H_{Pl}$ | Water head for unknown point (m) |
| $H_{Al}$,$H_{Bl}$ | Water head for given points (m) |
| $S_l$ | Wetted perimeter of liquid flow (m) |
| $S_g$ | Wetted perimeter of gas flow (m) |
| $S_i$ | Length of gas-liquid interface (m) |
| $P_0$ | Reference pressure (Pa) |
| $P_v$ | Vapor phase pressure (Pa) |
| $P_a$ | Pressure on the upstream face of the pig (Pa) |
| $P_b$ | Pressure on the downstream face of the pig (Pa) |
| $P_{max}$ | Maximum allowable hydrostatic pressure (MPa) |
| $P_{test}$ | Test pressure on the highest point (MPa) |
| $P_s$ | Hydrostatic pressure (MPa) |
| $Q_l$ | Volume rate of liquid ($m^3/s$) |
| $Q_{Pl}$ | Volume rate for unknown point ($m^3/s$) |
| $Q_{Al}$,$Q_{Bl}$ | Volume rates for given points ($m^3/s$) |
| $V_l$ | Liquid phase velocity (m/s) |
| $V_g$ | Gas phase velocity (m/s) |
| $V_{PIG}$ | Pig velocity(m/s) |
| $\tau_i$ | Shearing stress of gas-liquid interface (Pa) |
| $\tau_g$ | Shearing stress of gas phase (Pa) |
| $\tau_l$ | Shearing stress of liquid phase (Pa) |
| $\rho_l$ | Density of liquid ($kg/m^3$) |
| $\rho_m$ | The mean density ($kg/m^3$) |
| $\beta_0$ | Reference volumetric fraction of gas |
| $\sigma_h$ | Hoop stress (MPa) |
| $\sigma_s$ | Yield strength (MPa) |
| $\Delta P_k$ | The axial contact kinetic friction (Pa) |

## INTRODUCTION

With the wide application of pigging technology in the oil and gas industry, especially in the construction and operation of long-distance pipelines over undulating terrain, pipeline pigging technology has received more and more attention. The global long-distance oil and gas pipelines have reached 2,057,944.9 km, and 196,368 km are planned in the future (Wang *et al.* 2015). Before a new oil/gas pipeline goes into production, it is necessary to test its strength and tightness with the pipeline water pressure test. After the pressure test, the pipeline must be depressurized, and then an air compressor is used for gas injection. The fluid state of the pipeline changes continuously during the pigging process, which is a transient process. The pig pushes the liquid out of the pipe. When the pig is close to the end of the pipe, the pig quickly pushes the downstream liquid and the displacement increases significantly. As the speed of the water flow increases, its disturbance also increases. Meanwhile, the sludge at the bottom of the pipe will be discharged along with the water. The discharged water is first turbid and yellow, then the water quality returns to being clear, and there is a gas-liquid eruption at the end, as shown in Figure 1.

Even in the pigging process after the water pressure test of an undulating pipe, although the pipeline production process (such as the mechanical properties) and the operation process (such as the construction, the pressure test, and the pigging process) meet the specification requirements, the interaction of the medium inside the pipe can still cause instantaneous overpressure, which eventually leads to a pipe burst accident (Luo *et al.* 2011), as shown in Figure 2. So, it is necessary to study the transient pigging characteristics for the gas-liquid eruption and overpressure problems in the pigging process.

At present, researchers have carried out a lot of pigging experiments and numerical calculations. McDonald &

**Figure 1** | On-site vapor-liquid flow at the end of a pipeline.

**Figure 2** | The pipe rupture caused by abnormal overpressure (Deng *et al.* 2014).

Baker (1964) first proposed a model that can describe the pigging process of a gas-liquid two-phase flow pipeline. The model uses some steady-state processing methods, including liquid holdup and two-phase flow drop correlation. Barua (1982) improved the McDonald model but retained a steady-state model. Kohda *et al.* (1988) solved the pigging model based on a two-phase transient flow equation in a fixed coordinate system, which can predict the movement law of the pig. Minami & Shoham (1996) studied the quasi-steady-state pigging model in a fixed coordinate system in order to predict the position of the pig, the position of the liquid plug in front of the pig and the pressure difference before and after the plug. However, this model does not apply to the gas lift with a large amount of gas accumulation in front of the pig and the physical model of the ball clearing. Campo & Rachid (1997) first introduced the method of characteristics (MOC) into the pipeline pigging study. Azevedo *et al.* (2003) proposed the use of the finite difference method to simulate pigging under isothermal conditions, using steady-state assumptions and fluid incompressibility assumptions. Xu & Gong (2005) studied the pigging process of rich gas pipelines, and coupled the phase state model in the pigging simulation, which can simulate the transient process of the pigging process.

In order to accurately predict the actual operating state of the pigging process, researchers began to study the single-phase pigging process in the 1980s, and proposed different transient pigging models. Nguyen & Kim (2001) proposed the pig power model of the gas pipeline and the calculation method of the pig power model at the 90° elbow, using MOC strategy and a rectangular grid to predict the gas transient process in the pipeline. The Runge-Kutta iteration is also used to solve the dynamic equation of the pig. Esmaeilzadeh *et al.* (2009) proposed a non-steady-state pig model based on the Nguyen model, which is closer to the actual gas pipeline pigging process, and used the characteristic line method to solve the fluid equation and the Runge-Kutta mathematical method to solve the momentum equation of the pig. The model is able to predict the instantaneous pressure of the gas in the pipeline. Based on the previous model, the bypass model of the pipeline pig at constant temperature and high pressure was proposed (Hosseinalipour *et al.* 2007). Tolmasquima & Nieckele (2008) used the finite difference method to couple the motion equation of the pig, which can accurately predict the running speed of the pig.

It is observed that there is massive gas-liquid eruption at the outlet, forming a large gas-liquid column in the late stage of field pigging. Such phenomena are also described in the relevant literatures (Zhao *et al.* 2013). These papers analyze the hydraulic state of the pipe flow, and establish the liquid plug movement and the compressible fluid dynamics models. The influences of the development, propagation, and reflection of the water pressure wave on the fluid state in the pipe are described. However, the effects of the gas-liquid eruption are not taken into consideration based on the pig transient model. Figure 3 shows the pig entering the downdip pipe. The downdip pipe section close to the end accumulates gas within a certain range, thus forming slack flow. When the pig reaches a local high point, it will push the front air pocket and the liquid column downward at a high speed, and compress the air pocket enclosed in the downhill section, resulting in its pressure increase (Figure 3(a)). For a horizontal or slightly up-dip pipe, when the compressed cavitation moves near the end of the pipe's outlet, the gas collects at the top of the pipe and the liquid flows under the cavitation, forming a stratified flow with a smooth interface. As the liquid is further discharged, the gas accumulates at the top, the gas-liquid interface then develops to the outlet, and finally the cavitation will be connected to the outside atmosphere (Figure 3(b)). And since the pressure of the cavitation is much higher than the atmospheric pressure, the gas velocity will suddenly increase,

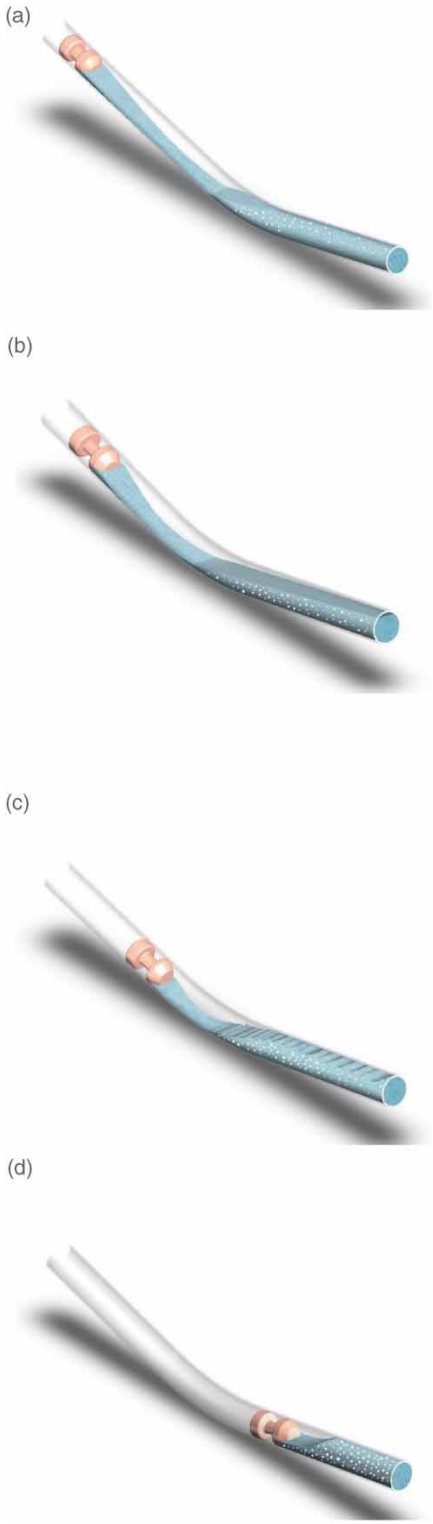


**Figure 3** | Diagram of vapor-liquid eruption: (a) the pig pushes the front air pocket and the liquid column downward at high speed; (b) the front air pocket is connected to the atmosphere; (c) impulse flow; (d) dispersed bubble flow.

forming a wavy flow at the gas-liquid interface. As the liquid is discharged, the resistance of the gas decreases gradually, while the speed is further increased; the waves are intensified, which can reach the upper part of the pipe wall, and then part of the liquid is carried away by the high-speed airflow forming an impulse flow (Figure 3(c)). When the airflow speed continues to increase and the liquid level reaches a certain height, the turbulent pulsation is intense under the disturbance of the high-speed airflow. The gas flowing at high speed tends to mix with the liquid flowing below, and the gas is dispersed into the fluid in the form of small bubbles. Finally, the flow pattern is converted into the dispersed bubble flow (Figure 3(d)). This entire process takes place in a very short period of time and eventually leads to a gas-liquid eruption.

Most of the existing pig power models are based on steady-state or quasi-steady-state assumptions, but in fact, the pig's movement is unsteady during the pigging process. Due to the compressibility of air, the pressure and flow changes can cause the motion state of the pig to change constantly. Hence the motion characteristics described by the steady-state pigging kinetic model are quite different from the actual ones, and the movement patterns of pigs cannot be accurately predicted. That is to say, the published transient models have their limitations and are not suitable for pigging calculations after the water pressure test. The theoretical studies on single-phase flow are relatively mature. However, little research has been done on the effects of pig movement on hydraulic transients during the drainage process, especially the instantaneous high-pressure mechanism of gas-liquid two-phase flow. For the study of the pigging process after a water pressure test of the undulating pipe, researchers have only adopted the pig power model, and simply combined the single-phase or multi-phase pipe flow characteristics to approximate the hydraulic characteristics of the pigging process. However, they have ignored the interaction between the kinetic characteristics of the pig and the hydraulic characteristics of the upstream and downstream fluids, which is crucial for studying the mechanism of instantaneous high-pressure generation during the drainage process. After the water pressure test, the hydraulic transient in the pigging process is complicated, and many influencing factors need to be taken into consideration, which increases the difficulty of establishing a mathematical model.

## MATHEMATICAL METHODS

In order to obtain the medium velocity and pressure field and the pig's movement in the pigging process, it is necessary to solve the fluid continuity equation, momentum equation, pig motion equation and the gas-liquid eruption model.

### Liquid equations and MOC

The fluid continuity equation is as follows:

$$\frac{\partial P}{\partial t} + V_l \frac{\partial P}{\partial x} + \rho_l \left(\frac{a^2}{A}\right) \frac{\partial Q_l}{\partial x} = 0 \tag{1}$$

The liquid motion equation is modeled as:

$$\frac{\rho_l}{A}\left(\frac{\partial Q_l}{\partial t} + V_l \frac{\partial Q_l}{\partial x}\right) + \frac{\partial P}{\partial x} + \rho_l g f Q_l |Q_l|^{1-m} = 0 \tag{2}$$

The friction coefficient $f$ is given by:

$$f = \frac{8\lambda Q_l^m}{g\pi^2 D^5} \tag{3}$$

Equations (4)–(6) represent expressions of $f$ under different flow patterns. For the region of laminar flow, $m$ is equal to 1.

$$f = 4.15 \frac{\nu}{D^4} \tag{4}$$

For the turbulent flow region, $m$ is equal to 0.25.

$$f = 0.0246 \frac{\nu^{0.25}}{D^{4.75}} \tag{5}$$

For the turbulent completely rough region, $m$ is equal to 0.

$$f = \frac{0.0826}{\left[2\lg\left(\frac{K}{3.71D}\right)\right]^2 D^5} \tag{6}$$

The calculation formula $f$ in the turbulent mixed region is complicated, and it is difficult to obtain the form of the Leapienzon formula. There are two approximate calculation formulas (Equations (7) and (8)).

For $m = 0.123$, $f$ is given by:

$$f = \frac{0.01893 \times K^{0.127} \nu^{0.123}}{D^{5.004}} \tag{7}$$

For $m = 0.125$, $f$ has the following form:

$$f = \frac{0.0188 \times K^{0.125} \nu^{0.125}}{D^{4.875}} \tag{8}$$

The general formula for the wave velocity of the pure liquid phase is used to calculate the velocity wave propagation velocity in the pipe flow.

$$a = \frac{1}{\sqrt{\rho_l \frac{1}{K} + \frac{D}{E\mathrm{e}}\psi}} \tag{9}$$

When the ratio $D/e$ of wall thickness to pipe diameter is small, the stress distribution on the pipe wall is uneven. Therefore, when $D/e$ is less than 25, Halliwell (1963) pointed out that the following situations need to be considered:

(1) One end of the pipe is fixed and the other end is not fixed:

$$\psi = \frac{2\mathrm{e}}{D}(1+\mu) + \frac{D}{D+\mathrm{e}}\left(1 - \frac{\mu}{2}\right) \tag{10}$$

(2) Both ends of the pipe are fixed and the axial direction cannot be extended:

$$\psi = \frac{2\mathrm{e}}{D}(1+\mu) + \frac{D}{D+\mathrm{e}}(1-\mu^2) \tag{11}$$

(3) The pipe can be freely stretched:

$$\psi = \frac{2\mathrm{e}}{D}(1+\mu) + \frac{D}{D+\mathrm{e}} \tag{12}$$

There are three main methods for the gas-liquid flow equation: MOC, the wave characteristics method, and the finite different method. Wylie & Streeter (1983) proposed MOC for solving the partial differential equation of transient

flow. This method can be used to analyze the unstable flow of the pipeline during the pigging process after the water test. First, the partial differential equation is transformed into the ordinary differential equation. Then the ordinary differential equation is transformed into a difference equation by mathematical methods.

Along the positive direction $C^+$, the partial differential equation can de written as:

$$\begin{cases} \dfrac{dx}{dt} = +a \\ \dfrac{a}{gA}dQ_l + dH + fQ_l|Q_l|^{1-m}adt = 0 \end{cases} \tag{13}$$

Along the reverse direction $C^+$, the partial differential equation can be written as:

$$\begin{cases} \dfrac{dx}{dt} = -a \\ \dfrac{a}{gA}dQ_l - dH + fQ_l|Q_l|^{1-m}adt = 0 \end{cases} \tag{14}$$

The finite difference method uses differential instead of differentiation to replace the difference equations, and then solves them to obtain an approximate solution.

As shown in Figure 4, on the grid plane, lines PA and PB are two characteristic lines of $+a$ and $-a$, respectively. Regardless of the problem of gas release and vaporization in the pipeline, or in the case of a small amount of vaporization, $a$ is regarded as a constant. Integrating the partial differential Equations (13) and (14) according to the positive characteristic line PA and the reverse characteristic line PB,

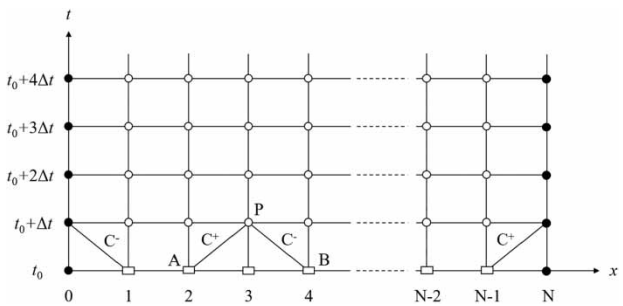


**Figure 4** | x-t plane computing grid for difference method. Rectangles: initial points; black dots: boundary nodes; circles: nodes within the boundary.

Equations (15) and (16) can be obtained:

$$C^+\begin{cases} \Delta x = a\Delta t \\ \dfrac{a}{gA}(Q_{Pl} - Q_{Al}) + (H_{Pl} - H_{Al}) + \displaystyle\int_A^P fQ_l|Q_l|^{1-m}dx = 0 \end{cases} \tag{15}$$

$$C^-\begin{cases} \Delta x = -a\Delta t \\ \dfrac{a}{gA}(Q_{Pl} - Q_{Bl}) - (H_{Pl} - H_{Bl}) + \displaystyle\int_B^P fQ_l|Q_l|^{1-m}dx = 0 \end{cases} \tag{16}$$

For accuracy and convenience of calculation, the approximate calculation method by Streeter & Wylie (1967) is used to calculate the hydraulic friction term.

For the $A$-$P$ section,

$$Q_l|Q_l|^{1-m} = Q_{Pl}|Q_{Al}|^{1-m} \tag{17}$$

For the $B$-$P$ section,

$$Q_l|Q_l|^{1-m} = Q_{P_l}|Q_{Bl}|^{1-m} \tag{18}$$

Therefore, the finite difference equations for the approximate hydraulic transient characteristic equation can be written as follows:

$$C^+\begin{cases} \dfrac{\Delta x}{\Delta t} = +a \\ \dfrac{a}{gA}(Q_{Pl} - Q_{Al}) + (H_{Pl} - H_{Al}) + fQ_{Pl}|Q_{Al}|^{1-m}a\Delta t = 0 \end{cases} \tag{19}$$

$$C^-\begin{cases} \dfrac{\Delta x}{\Delta t} = -a \\ \dfrac{a}{gA}(Q_{Pl} - Q_{Bl}) - (H_{Pl} - H_{Bl}) + fQ_{Pl}|Q_{Bl}|^{1-m}a\Delta t = 0 \end{cases} \tag{20}$$

Based on Equations (19) and (20), the following equations can be obtained:

$$C^+: H_{Pl} = R_{Al} - S_{Al}Q_{Pl} \tag{21}$$

$$C^-: H_{Pl} = R_{Bl} + S_{Bl}Q_{Pl} \tag{22}$$

where $R_{Al}$, $R_{Bl}$, $S_{Al}$, and $S_{Bl}$ are given by

$$R_{Al} = H_{Al} + C_{Wl}Q_{Al} \tag{23}$$

$$R_{Bl} = H_{Bl} - C_{Wl}Q_{Bl} \tag{24}$$

$$S_{Al} = C_{Wl} + f|Q_{Al}|^{1-m}a\Delta t \tag{25}$$

$$S_{Bl} = C_{Wl} + f|Q_{Bl}|^{1-m}a\Delta t \tag{26}$$

$C_{Wl}$ is given by:

$$C_{Wl} = \frac{a}{gA} \tag{27}$$

Equation (28) can be calculated according to Equations (21) and (22):

$$Q_{Pl} = \frac{R_{Al} - R_{Bl}}{S_{Al} + S_{Bl}} \tag{28}$$

Finally, $H_{pl}$ can be obtained by substituting $Q_{pl}$ into Equation (21) or Equation (22).

## Pig motion equation

Two-way straight pipe pigs are generally used in the pigging operation after the water pressure test. They are sealed because of the interference of the sealing disc against the pipe. Due to the differential pressure between the front and the rear, the pigs are able to move downstream to drain and can be used repeatedly. The pig is subjected to four forces: gravity, the upstream gas driving force, the downstream reverse hydraulic pressure, and the friction resistance between the pig and the wall.

$$P_a = P_b + \Delta P_k + \frac{1}{A}M \cdot g \cdot \sin\alpha + \frac{M}{A}\frac{dV_{PIG}}{dt} \tag{29}$$

Unlike the steady-state calculation, the pig's speed in the pigging process is not preset in the transient pigging calculation because it is difficult to control in practice. The key to establishing a transient pigging model is to find the position of the pig at each time step to track the pig. The Euler-Lagrange method is adopted to calculate the boundary motion of the pig. For the upstream and downstream media that are completely blocked by the pig, the flow equation is solved by MOC strategy on a fixed double grid. Combined with the pig power model, the pig speed can be obtained. Substituting the pig speed into the medium flow relationship to obtain a new pressure iteratively solves it until the preset accuracy is met. The pigging speed can be figured out once the iteration terminates.

## Vapor-liquid eruption model

The vapor-liquid phases are thoroughly mixed under strong disturbance, so they can be treated as single-phase medium to deal with two-phase fluid kinetic problems. The homogeneous flow model has higher accuracy in dealing with the flow of such homogeneous mixed media.

(1) The velocity of the gas and the liquid are the same, and thus the slip between phases is 0.
(2) The two-phase medium is in a state of kinetic equilibrium, and the pressure of the gas and the liquid are the same.
(3) The two-phase medium is in a thermodynamic equilibrium state. This state is valid in isothermal fluids.

For an unsteady one-dimensional homogeneous equilibrium flow in horizontal or near-horizontal tubes, the basic equation can be expressed as:

$$\frac{\partial\rho_m}{\partial t} + \frac{Q}{A}\frac{\partial\rho_m}{\partial x} + \frac{\rho_m}{A}\frac{\partial Q}{\partial x} = 0 \tag{30}$$

$$\frac{1}{gA}\left(\frac{\partial Q}{\partial t} + \frac{Q}{A}\frac{\partial Q}{\partial x}\right) + \frac{1}{\rho_m g}\frac{\partial P}{\partial x} + fQ|Q|^{1-m} = 0 \tag{31}$$

Since the gas phase density is much smaller than the liquid phase density, the influence of the gas phase density can be ignored. The average density of the medium is represented by $\rho_m$, which can be expressed as:

$$\rho_m = (1-\beta)\rho_l \tag{32}$$

When the gas phase and the liquid phase are in equilibrium, the gas is dispersed in the liquid phase in the form of small bubbles. Therefore, the relationship between

volumetric gas content and pressure can be expressed as:

$$\beta = \frac{1}{1 + \frac{P - P_v}{P_0}\left(\frac{1}{\beta_0 - 1}\right)} \tag{33}$$

MacCormack (2003) proposed a discrete method for hyperbolic partial differential equations, which is a finite difference form with second-order accuracy. Because of its simple application, this method is widely used in the field of computational fluid dynamics. The method is applied to the above equations in two steps: prediction and correction.

(1) Prediction

The spatial derivative of the continuity Equation (31) adopts the method of forward difference, and can be modeled as:

$$\left(\frac{\partial \rho_m}{\partial t}\right)_{i,j}^{t} = -\frac{Q_i^t}{A\Delta x}(\rho_{m,i+1}^t - \rho_{m,i}^t) - \frac{\rho_{m,i}^t}{A\Delta x}(Q_{i+1}^t - Q_i^t) \tag{34}$$

All variables in Equation (34) are known parameters. So $\left(\frac{\partial \rho_m}{\partial t}\right)_{i,j}^{t}$ is known. The predicted density obtained by the Taylor series method can be expressed as:

$$(\bar{\rho}_m)_i^{t+\Delta t} = \rho_{m,i}^t + \left(\frac{\partial \rho_m}{\partial t}\right)_i^t \Delta t \tag{35}$$

The predicted value of density $(\bar{\rho}_m)_i^{t+\Delta t}$ is only a first-order accuracy, because only the liner terms in the Taylor expansion are included.

In the same way, the predicted value of the flow can be obtained.

$$(\bar{Q})_i^{t+\Delta t} = Q_i^t + \left(\frac{\partial Q}{\partial t}\right)_i^t \Delta t \tag{36}$$

(2) Correction

The predicted value is substituted into the continuity equation, and the spatial derivative is gained by the backward difference method.

$$\left(\overline{\frac{\partial \rho_m}{\partial t}}\right)_i^{t+\Delta t} = -(\bar{\rho}_m)_i^{t+\Delta t}\frac{(\bar{Q})_i^{t+\Delta t} - (\bar{Q})_{i-1}^{t+\Delta t}}{A\Delta x} + (\bar{Q})_i^{t+\Delta t}\frac{(\bar{\rho}_m)_i^{t+\Delta t} - (\bar{\rho}_m)_{i-1}^{t+\Delta t}}{A\Delta x} \tag{37}$$

Thus, we can get the arithmetic mean of the density and the arithmetic mean of the flow.

$$\left(\frac{\partial \rho_m}{\partial t}\right)_{av} = \frac{1}{2}\left[\left(\frac{\partial \rho_m}{\partial t}\right)_i^t + \left(\overline{\frac{\partial \rho_m}{\partial t}}\right)_i^{t+\Delta t}\right] \tag{38}$$

Similarly,

$$\left(\frac{\partial Q}{\partial t}\right)_{av} = \frac{1}{2}\left[\left(\frac{\partial Q}{\partial t}\right)_i^t + \left(\overline{\frac{\partial Q}{\partial t}}\right)_i^{t+\Delta t}\right] \tag{39}$$

The corrected value of density at time $t + \Delta t$ is:

$$\rho_{m,i}^{t+\Delta t} = \rho_{m,i}^t + \left(\frac{\partial \rho_m}{\partial t}\right)_{av} \Delta t \tag{40}$$

Using the same method, the correction value of the flow is available at time $t + \Delta t$:

$$Q_i^{t+\Delta t} = Q_i^t + \left(\frac{\partial Q}{\partial t}\right)_{av} \Delta t \tag{41}$$

Substituting $\rho_{m,i}^{t+\Delta t}$ into Equation (32) to get $\beta_i^{t+\Delta t}$, and then substituting it into Equation (33) to get $P_i^{t+\Delta t}$.

Since stratified flow appeared at the end of the pipeline before the gas-liquid eruption occurred, the stratified flow analysis model was used to obtain the initial parameters of the eruption calculation. Taitel & Dukler (1976) performed a mechanical analysis of the stratified flow in horizontal and near-horizontal pipe flow. The results show that in the case of medium-high liquid phase load and low flow rate, it can be approximated that the interface between the gas and liquid phases is flat (as shown in Figure 5), and there are no entrained droplets in the gas flow. The momentum change caused by mass exchange between gas and liquid phase was not considered.

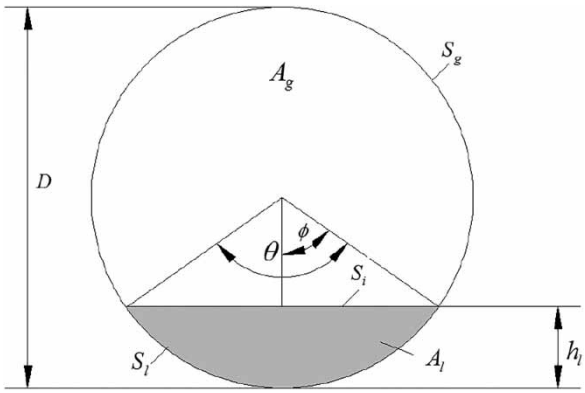


**Figure 5** | Geometric relationship of cross-section parameters for stratified flow.

Equations (42) and (43) represent the gas momentum equation and the liquid momentum equation, separately.

$$-A_g\frac{dp}{dx}-\rho_g g A_g\sin\alpha-\tau_i S_i-\tau_g S_g=0 \tag{42}$$

$$-A_l\frac{dp}{dx}-\rho_l g A_l\sin\alpha+\tau_i S_i-\tau_l S_l=0 \tag{43}$$

The pressure gradient term in the gas and liquid phase momentum equations are eliminated to obtain the following combined momentum equation (also known as the liquid holdup equation, or slippage relationship).

$$-\frac{\tau_l S_l}{A_l}+\frac{\tau_g S_g}{A_g}+\tau_i S_i\left(\frac{1}{A_l}+\frac{1}{A_g}\right)-(\rho_l-\rho_g)g\sin\alpha=0 \tag{44}$$

where $\tau_l$, $\tau_G$and, $\tau_i$ are given by:

$$\tau_l=\frac{1}{2}f_l\rho_l V_l|V_l| \tag{45}$$

$$\tau_G=\frac{1}{2}f_G\rho_G V_G^2 \tag{46}$$

$$\tau_i=\frac{1}{2}f_i\rho_g(V_g-V_l)|V_g-V_l| \tag{47}$$

## RESULTS AND DISCUSSION

In the pipeline where the pipe burst occurred, the pipe length for the pigging operation is 6.971 km. The gas injection point (point A), with an elevation of 737.18 m, is the highest point. In addition, the bottom of the V-shaped gully (point C) has an elevation of 573.9 m. The lowest point of the whole line (point E) is 558 m. The end drain valve (point F), with an elevation of 561.94 m, has a maximum height difference of 178.8 m, which is a typical undulating terrain, as shown in Figure 6. The parameters, such as on-site pipelines, pigs, and compressors, are shown in Table 1.

In the fourth stage, the pig reaches the end of the pipe. The pipe section between point E (the bottom of the downhill section) and point F (the drainage outlet) is slightly inclined upwards, which the conditions of the gas-liquid

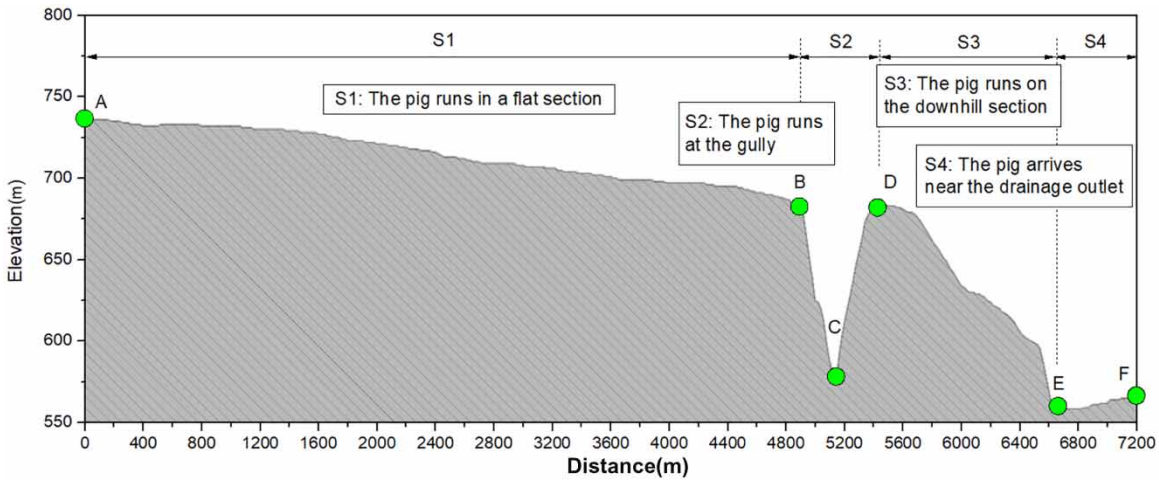


**Figure 6** | Elevation profile of pipeline with the first accident.

**Table 1** | Summary of basic parameters for field operations

| Parameters | Values |
|---|---|
| Pipe length | 6.971 km |
| Maximum height difference | 178.8 m |
| Pipe specification | $\Phi$1,219 × 18.4 mm |
| Pig quality | 700 kg |
| Static friction resistance between pig and pipe wall | 0.04 MPa |
| Dynamic friction resistance between pig and pipe wall | 0.03 MPa |
| Air compressor type | XHP1070 |
| Rated pressure | 2.2 MPa |
| Rated flow rate | 0.5 $Nm^3/s$ |

eruption analyzed above, triggering a violent interaction between the gas and liquid and the water hammer, thus resulting in a sudden increase in pressure. Therefore, part of the retained liquid and the gas accumulated at the front end of the pig erupted under the pig's movement.

The design strength of the pipe section is 12.5 MPa, the tightness test pressure is 10 MPa, and the pressure test medium is water. According to the relevant specifications, in general, the hoop stress of the pipe should not exceed 0.9 times the minimum yield strength of the pipe, as in Equation (48). The instantaneous pressure in the tube at the time of bursting is at least PB, according to Equations (48)–(50). The yield strength of X80 steel is 690 MPa. Consequently, the X80 pipe PB with a wall thickness of 18.4 mm is 20.83 MPa. The maximum allowable hydrostatic pressure $P_{\max}$ for the pipeline is 18.74 MPa. In view of the design requirements, the highest test pressure $P_{\text{test}}$ is 12.5 MPa, and the hydrostatic pressure $P_s$ in the pipe is 6.24 MPa, which is converted to a water column with a height of 636.7 m. Therefore, the division result of this pipe segment conforms to the principle of segmentation pressure test division, and the hydrostatic head does not harm the pipeline's safety.

$$\sigma_h = P_{\max} \times D_e/(2\delta) \leq 0.90\sigma_s \tag{48}$$

$$P_B \times D_e/(2\delta) = \sigma_s \tag{49}$$

$$P_{\max} = P_{test} + P_s \tag{50}$$

However, after the pressure test of segmental pigging, a burst accident occurred in both pigging operations. The information about the two accidents is shown in Table 2. The first pigging operation was performed on July 19, after the completion of the pressure test and the, two air compressors and DN150 drain valve had been installed. After all the processes were ready, the pig was then placed in the pipeline. The compressor started at 9:00 am and the drain valve was opened at the same time. At 5:00 pm the next day, the gas-liquid eruption was observed at the pipe outlet. At that time, the pig had been running for 20 hours and a 2.6 m fracture was found in the last section of the pipeline. The second pigging operation was carried out on September 21, and an air compressor and a DN150 drain valve were installed. After all the processes were completed, the pig was placed in the pipeline. The compressor was started at 3:00 am and the drain valve was opened at the same time. At 6:30 pm the next day, the second pipe burst occurred and another 2.5 m new break was found at a distance of 5 m from the first break. According to the recorded data, the maximum pressure of compressed air was 1.03 MPa in this process. But there were no quality defects in the pipe segment through the investigation. The rated pressure of the air compressor is 2.2 MPa, so it is unlikely to have caused the damage to the pipe, as shown in Table 2.

## The first accident

Two accidents were simulated by using the pigging transient simulation program proposed in this paper. Figure 7 shows the pressure change at the gas injection end (point A) in the pigging process. It can be seen that in the initial stage, after the gas injection pressure reaches 0.09 MPa, the pig can overcome the resistance downstream reverse hydraulic

**Table 2** | Summary of the two accidents

| Parameters | First accident | Second accident |
|---|---|---|
| Pressure when the pipe burst | 20.83 MPa | 20.83 MPa |
| Piping time | 20 hours | 39.5 hours |
| Number of gas injection compressors | 2 | 1 |
| Maximum air pressure | | 1.01 MPa |
| Drainpipe specifications | $\Phi$159.0 × 8.7 mm | $\Phi$159.0 × 8.7 mm |
| Length of rupture | 2.6 m | 2.5 m |

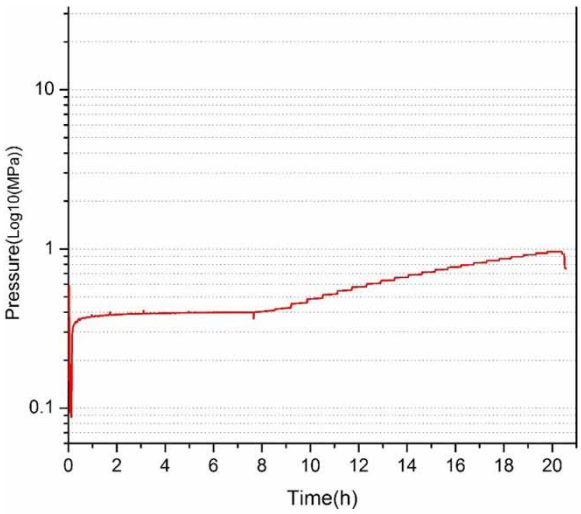


**Figure 7** | Numerical result of pressure at point A for the first accident.

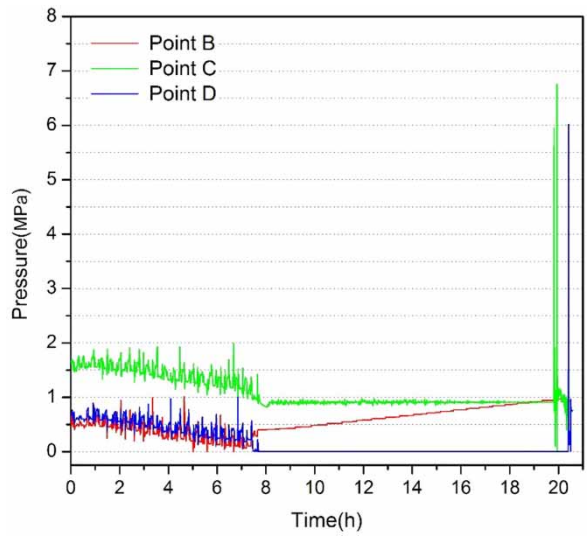


**Figure 8** | Numerical result of pressure at points B, C and D for the first accident.

resistance and its friction resistance with the pipe wall to move. When the pig is operated in a flat section, the pressure at the gas injection end tends to be stable, and its value fluctuates around 0.39 MPa. After the 8th hour, the pig enters the gully operation stage. The pig moves very slowly. As the compressed gas is continuously injected, the pressure at the gas injection end increases. When the pressure is increased to 1.01 MPa, the pig reaches the bottom of the gully, followed by a sharp drop in pressure until the pipe eventually bursts. The pressure at the drain end slowly decreases from 0 to 8 hours. According to the site situation, the degree of opening of the drain valve was initially controlled in order to ensure the safety of the drainage, resulting in the slow pace of the drainage. Simultaneously, the pig moves relatively smoothly downstream, so that the liquid in the downhill section near the outlet accumulates in time, and the liquid level does not drop.

The pig passes point B at 8 hours (as shown in Figure 8). After that, the pressure at point B is equal to the gas pressure. The pressure at point C is maintained at a level of 1.01 MPa due to the hydrostatic head caused by the height difference (point C at the bottom of the gully and local high point D at the downstream). Its pressure reaches a maximum of 6.7 MPa before the pig passes through point C. The pressure at the local high point D first reaches the saturated vapor pressure, and vaporization occurs and remains for a long time. The pig passes the highest point D with a maximum pressure of 6.1 MPa.

After the pig enters the gully movement, the pig's movement slows down. At this time, the liquid level in the downhill section begins to drop, and the pressure at the drain end drops faster. The end pressure is maintained at a very low level after 10 hours (Figure 9). This state is maintained for a long time, and as the liquid level of the downhill section increases, the end pressure would increase slightly. Finally, the pig maintains high-speed motion near the drain. The front liquid plug and the liquid accumulated in the end of the pipeline violently collide and cause a

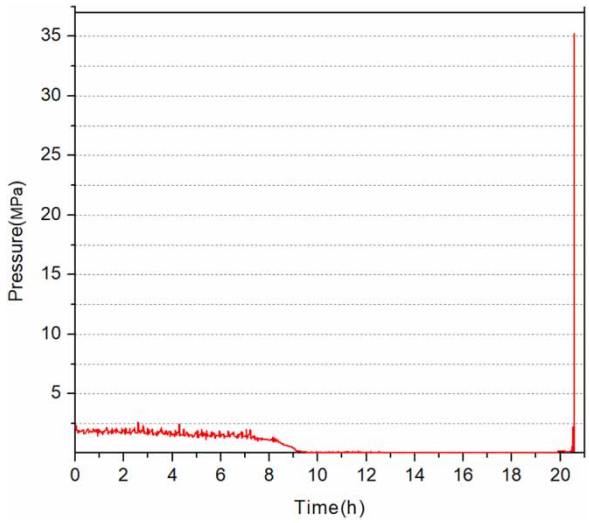


**Figure 9** | Numerical result of pressure at point F for the first accident.

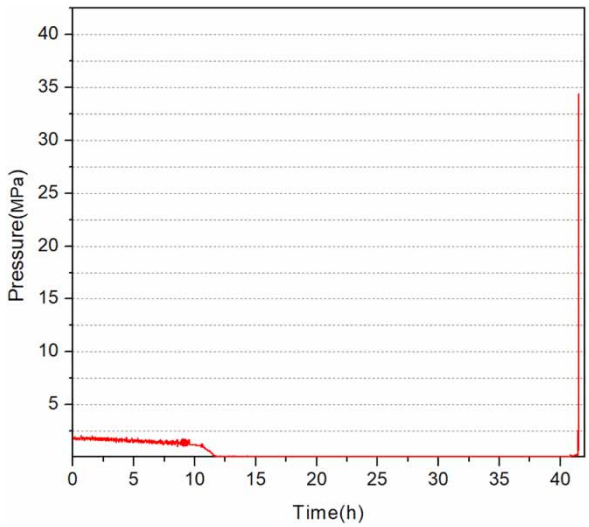


**Figure 10** | Numerical result of pressure at point F for the second accident.

hydraulic pulse. The instantaneous pressure (35.2 MPa) far exceeds the ultimate bearing pressure of the pipeline (20.83 MPa), which causes the burst to occur.

### The second accident

The numerical simulation of the second on-site pigging was carried out. In the case of only one air compressor, the overall length of pigging is longer, up to 41.5 hours, due to the reduced gas injection flow, and the operation of the pig in the flat section is extended to 10 hours. The maximum pressure at the bottom of the gully (point B) is only 6.5 MPa. In the final overpressure stage (when the pig reaches the drain), the instantaneous speed is 19.2 m/s, which is lower than when two air compressors are used for pigging. In the case of using only one air compressor, the instantaneous overload pressure (34.4 MPa) is also generated at the end of the pipe in the last period, resulting in a burst, as shown in Figure 10.

### Comparison of field result and simulating result

The comparison of field data and the simulation results is shown in Table 3. The first pigging process took 20 hours on site and the calculated result is 20.5 hours. The second pigging process took 39.5 hours on site while the calculated result is 41.5 hours. The relative errors of these two are 2.5% and 5.0%, respectively. The maximum pressure at the gas injection end is 1.03 MPa, yet the calculation pressure at the gas injection end of the two piggings is 1.01 MPa. The maximum number of hydraulic pulses was not recorded in either of the two pipe burst accidents. According to theoretical calculations, the minimum pressure at which the squib occurs is 20.83 MPa. The maximum hydraulic impulses of the two pigging simulations were 35.2 MPa and 34.4 MPa, respectively, which were 169 and 165% of the safety pressure. The second pigging on-site operation uses a method of reducing inlet flow. Although the maximum value of the hydraulic pulse is reduced, its value far exceeds the ultimate bearing pressure of the pipe, and the occurrence of a pipe burst accident cannot be avoided.

## CONCLUSION

It is possible to determine the dynamic parameters of the pipeline and obtain the pulse pressure of the two accidents by using the proposed model. The pig quickly pushes the downstream liquid and compresses the end gas when the pig is near the end of the pipe. The bubble collapse caused the pulse pressure, followed by a gas-liquid eruption, which led to a serious pipe burst accident during pigging. The numerical simulation results show that the predicted values of the model are consistent with the field data. In general, the topographical fluctuations of the pipeline are a key factor in determining

**Table 3** | Comparison between field data and calculated results

| | Field data for first accident | Calculated value for first accident | Field data for second accident | Calculated value for second accident |
|---|---|---|---|---|
| Time of pigging | 20 hours | 20.5 hours | 39.5 hours | 41.5 hours |
| Maximum pressure of gas injection end | 1.03 MPa | 1.01 MPa | 1.03 MPa | 1.01 MPa |
| Maximum pressure of gully bottom | / | 6.7 MPa | / | 6.5 MPa |
| Maximum of hydraulic pulse | $\geq$ 20.83MPa | 35.2 MPa | $\geq$ 20.83MPa | 34.4 MPa |

the state of liquid flow. Slope pipelines are most likely to have slack flow. Liquid column separation is a common phenomenon in undulating pipelines, which can have serious effects on pipeline safety, such as explosion accidents. Therefore, it is extremely important to take precautionary measures for pipeline safety during the pigging process. When there is an air pocket in the liquid phase of the pipeline, a high-pressure hydraulic pulse would be generated under the movement of the pig, the maximum value of which is greater than the gas injection pressure, and the instantaneous high pressure may endanger the safety of the pipeline. Therefore, a trapped air pocket should be avoided as much as possible during the pigging process after the water pressure test.

## ACKNOWLEDGEMENTS

The authors would like to express sincere thanks to the National Natural Science Foundation of China (51704253) for the financial support in this project.

## CONFLICT OF INTERESTS

The authors declare that there is no conflict of interests regarding the publication of this paper.

## DATA AVAILABILITY STATEMENT

All relevant data are included in the paper or its Supplementary Information.

## REFERENCES

Azevedo, L. F. A., Braga, A. M. B. & Nieckele, A. O. 2003 *Simulating Pipeline Pigging Operations*. Clarion Technical Publishers, Houston, TX, pp. 79–107.

Barua, S. 1982 *An Experimental Verification and Modification of the McDonald and Baker Pigging Model for Horizontal Flow. Ph.D. Dissertation*, University of Tulsa, Texas.

Campo, V. & Rachid, F. B. 1997 Modeling of pig motion under transient fluid flow. In *Proc. XIV Brazilian Congress of Mechanical Engineering-COBEM*, Sao Paulo, Brazil.

Deng, T., Gong, J., Yu, D., Wu, H. H., Yao, Y. N., Chen, X. & Zhou, J. 2014 Influence of complicated topography on pressure test and drainage of long distance gas pipelines. *Gas Storage and Transportation* **33** (12), 1326–1330 (in Chinese).

Esmaeilzadeh, F., Mowla, D. & Asemani, M. 2009 Mathematical modeling and simulation of pigging operation in gas and liquid pipelines. *Journal of Petroleum Science and Engineering* **8** (6), 1–7.

Halliwell, A. R. 1963 Velocity of water hammer wave in an elastic pipe. *Journal of the Hydraulics Division* **89**, 1–21.

Hosseinalipour, S. M., Zarif Khalili, A. & Aalimi, A. 2007 Numerical simulation of pig motion through gas pipelines. In *16th Australasian Fluid Mechanics Conference*. University of Queensland, Australia.

Kohda, K., Suzukawa, Y. & Furukwa, H. 1988 A new method for analyzing transient flow after pigging scores well. *Oil and Gas Journal* **86** (29), 40–47.

Luo, J. H., Yang, F. P., Ma, Q. R., Zhao, X. W., Wei, J. J. & Wang, H. T. 2011 Cause analysis of pressure test and drainage explosion of newly built large drop pipe. *Gas Storage and Transportation* **30** (6), 441–444 (in Chinese).

MacCormack, R. W. 2003 The effect of viscosity in hypervelocity impact cratering. *Journal of Spacecraft & Rockets* **40** (5), 27–43.

McDonald, A. & Baker, O. 1964 Multiphase flow in (gas) pipelines. *Oil and Gas Journal* **62** (24), 68–71.

Minami, K. & Shoham, O. 1996 Pigging dynamics in two-phase flow pipe lines: experiment and modeling. *International Journal of Multiphase Flow* **22** (1), 145–146.

Nguyen, T. T. & Kim, S. B. 2001 Modeling and simulation for PIG flow control in natural gas pipeline. *KSME International Journal* **15** (8), 1165–1173.

Streeter, V. L. & Wylie, E. B. 1967 *Hydraulic Transients*. McGraw-Hill Book Company, New York.

Taitel, Y. & Dukler, A. E. 1976 A theoretical approach to the Lockhart-Martinelli correlation for stratified flow. *International Journal of Multiphase Flow* **2** (5), 591–595.

Tolmasquima, S. T. & Nieckele, A. O. 2008 Design and control of pig operations through pipelines. *Journal of Petroleum Science and Engineering* **62**, 102–110.

Wang, H. J., Zhu, Q. Z. & Zhang, Y. P. 2015 Overview of global oil and gas pipeline construction. *Oil & Gas Storage and Transportation* **34** (1), 15–18.

Wylie, E. B. & Streeter, V. L. 1983 *Fluid Transients*, 2nd edn. Prentice Hall, Englewood Cliffs, NJ.

Xu, X. X. & Gong, J. 2005 Pigging simulation for horizontal gas-condensate pipelines with low-liquid loading. *Journal of Petroleum Science & Engineering* **48** (3), 272–280.

Zhao, G. H., Zheng, L., Zhao, H. R., Deng, X. & Jiang, F. G. 2013 Failure analysis of high-drop pipeline in the process of dewatering. *Engineering Failure Analysis* **33**, 139–150.

First received 6 August 2020; accepted in revised form 27 October 2020. Available online 11 November 2020